Electrochemical reduction of oxygen on nanoparticulate gold electrodeposited on a molecular template

Mirkhalaf, F. , Tammeveski, K. and Schiffrin, D.J.

Original citation & hyperlink:
Mirkhalaf, F. , Tammeveski, K. and Schiffrin, D.J. (2009) Electrochemical reduction of oxygen on nanoparticulate gold electrodeposited on a molecular template. Physical Chemistry Chemical Physics, volume 11 (18): 3463-3471.
http://dx.doi.org/10.1039/B818439A

Electrochemical reduction of oxygen on nanoparticulate gold electrodeposited on a molecular template

Fakhradin Mirkhalaf[*a,b], Kaido Tammeveski[c] and David J. Schiffrin[a]

[a]*Chemistry Department, University of Liverpool, Liverpool, L69 7ZD, UK*

[b]*Sonochemistry Centre, Coventry University, Coventry,CV1 5FB, UK*

[c]*Institute of Chemistry, University of Tartu, Jakobi 2, 51014 Tartu, Estonia*

*Corresponding author, Tel.: +44-2476888075; Fax: +44-2476888173; e-mail: famir@coventry.ac.uk

Abstract

The reduction of oxygen on gold electrodeposited on an organic template has been investigated. The template consisted of reduced 4-nitrophenyl groups attached to glassy carbon (GC) by the electrochemical reduction of the corresponding diazonium compound. The electrode modified by this Au nanostructured film shows electrocatalytic properties for the oxygen reduction reaction (ORR) different from those of bulk Au, GC or GC grafted with 4-nitrophenyl groups. The reduced nitrophenyl film inhibits the O_2 reduction reaction. A two-step reduction mechanism with production of hydrogen peroxide in the first step and water in the second was observed in alkaline solutions. The standard heterogeneous rate constants for this EE reduction mechanism have been calculated using non-linear regression analysis (NLR).

Key words: Electrocatalysis, Oxygen Reduction, Gold nanostructures, Templated Deposition, Hydrogen Peroxide production

1. Introduction

There has been an increased interest in the use of nanosized particles of metals and alloys as electrocatalysts since these present a much higher catalytic activity than bulk materials due to their large surface area and the presence of reactive surfaces sites .[1,2] Moreover, their catalytic properties are strongly dependent on their size and shape.[3,4] Electrocatalysts made from size and shape-controlled metal nanoparticles are being developed for the efficient and selective control of electrochemical reactions for example, for the electrocatalytic reduction of oxygen of importance in fuel cell technology.[1] Nanoparticles can be attached to an electrode surface by either chemical bonding or physical attachment and by controlled electrodeposition. The preparation of metal nanoparticles and/or nanostructured surfaces by electrodeposition has the advantage of simplicity, low cost and also, decreasing the risk of contamination during preparation.[5-7] In order to reduce oxygen selectively and efficiently on noble metals deposited

on an electrode, the deposition process must provide control of metal particle size and geometry.[4] The present work has attempted to modify deliberately the substrate surface to control the size of the electrodeposited nanostructures.

Nanostructured electrocatalysts have been previously prepared by chemical reduction of metal ions coordinated to an amino terminated film attached to HOPG[8] and by electrodeposition. For the latter, Pt,[9] Ag[10] and Pd[11] nanoparticles have been grown on organic functionalised carbon nanotubes and/or carbon electrodes for O_2 reduction or methanol oxidation. Boron-doped diamond (BDD),[12,13] Au,[14] Pt[15] and glassy carbon (GC)[16] have been used as substrates for electrodeposited gold. There has been recently interest in templated deposition as a means of controlling size and shape of nanostructures.[17-20] and organic monolayers have been investigated as templates.[9,11, 21-23] Significant improvements in the uniform deposition of metal nanoparticles were reported when suitable organic monolayers were attached to the electrode surface prior to deposition. For instance, nanoparticles of Pd[21] and Pt[22] have been grown on self-assembled monolayers (SAMs) chemisorbed on Au electrodes and nitrophenyl monolayers have been used as a template for the deposition of Pt,[9] Ag[10] and Pd[11] nanoparticles on multi-walled carbon nanotubes. Electrodeposition of Au on Pt(111) modified with a layer of benzenethiol and 1,2-benzenedithiol has also been reported.[23] The deposition of three-dimensional gold clusters was observed for the former.

The electrochemical reduction of oxygen follows two main pathways: a "direct" 4-electron reduction leading to water or OH^- ions in acid and alkaline solutions, respectively, and/or a pathway involving the formation of hydrogen peroxide as an intermediate. The peroxide formed can be further reduced following chemical/electrochemical mechanisms or it can disproportionate.[24-27] Which of these reaction channels is followed depends greatly on the electrode material and/or its crystal orientation and therefore, on the coordination of adsorbed oxygen.[24] Gold can supports both two- and four-electron pathways depending on surface orientation and experimental conditions.[24-27]

The purpose of the present work was to investigate the reduction of oxygen on nanostructured gold surfaces formed by electrodeposition through a nitrophenyl film used as a template

through which gold was electroplated. Grafting of the film to a glassy carbon electrode was achieved by the reductive cycling of the corresponding diazonium compound, a technique that has been extensively employed for the surface modification of carbon materials and metals with different functional groups.[28-32] It was of interest to investigate if templated electrodeposits could direct the reduction of oxygen in a different way from that of the bulk metal.[9-20]

2. Experimental

2.1. Chemicals

4-Nitrobenzenediazonium tetrafluoroborate (NBD, 97%, Aldrich), hydrogen tetrachloroaurate (III) trihydrate ($HAuCl_4 \times 3H_2O$, 99.9+%, Aldrich) and tetrabutylammonium tetrafluoroborate ($TBABF_4$, 99%, Aldrich) were used without further purification. Acetonitrile (HPLC grade, 99.93%, Aldrich) was stored over activated molecular sieves. Potassium hydroxide was from BDH (AnalaR); oxygen (99.95%) and Ar (99.997%) were obtained from BOC gases (UK). MilliQ® water (Millipore, Inc.) was used throughout.

2.2. Electrochemical measurements

A Pine Instrument Company glassy carbon (GC)-Au disk-ring electrode of 0.164 cm^2 disk area was employed. For the measurements in alkaline solutions, the ring potential was set at 0.0 V to ensure quantitative detection of the peroxide produced on the disk. A collection efficiency of 0.22 was determined from measurements of hexacyanoferrate(III) reduction. The electrode was polished to a mirror finish using increasingly finer aqueous alumina slurries (1.0, 0.3 and 0.05 μm, Buehler) prior to each experiment, followed by repeated sonication in water. The electrode was finally dried in a stream of high purity argon before surface modification. All experiments were performed in a three-electrode glass cell with a platinum gauze counter electrode and a saturated calomel reference electrode (SCE); all potentials are referred to this electrode. The potential was controlled with an Autolab PGSTAT20 potentiostat (Eco Chemie B.V., The Netherlands). The working electrode was rotated using a Pine Instrument Company (Grove City, PA, USA) AFMSRX rotator and MSRX speed controller. All measurements were made at room temperature (21 ± 1 °C). Non-linear regression analysis fits were performed using Microcal™ Origin® Version 7.0.

The O_2 reduction results were analysed using the Koutecky-Levich relationship:[33]

$$\frac{1}{I} = \frac{1}{I_k} + \frac{1}{I_d} = -\frac{1}{nFAkc_{O_2}^b} - \frac{1}{0.62nFAD_{O_2}^{2/3}\nu^{-1/6}c_{O_2}^b\omega^{1/2}} \quad (1)$$

where I is the measured current, I_k and I_d are the kinetic and diffusion-limited currents, respectively, n is the number of electrons transferred per O_2 molecule, k is the rate constant for O_2 reduction, F is the Faraday constant (96485 C mol^{-1}), A is the electrode area, ω is the angular rotation velocity (in rad s^{-1}), $c_{O_2}^b$ is the bulk oxygen concentration (1.21×10^{-6} mol cm^{-3}),[34] D_{O_2} is the diffusion coefficient (1.87×10^{-5} cm^2 s^{-1})[35] and ν is the kinematic viscosity of the solution (0.01 cm^2 s^{-1}).[36] The potential dependence of n was calculated from the slopes of these plots.

2.3. AFM and XPS measurements

Tapping mode AFM images were obtained with an STM/AFM (PicoScan 2000®, Molecular Imaging) equipment using PicoScan® software Version 4.1g and magnetically coated Si cantilevers. XPS measurements were carried out with a SCIENTA SES-100 spectrometer using a Mg Kα X-ray source (incident energy = 1253.6 eV) and a take-off angle of 90°. The following parameters were used for the survey scan: energy range = 900–0 eV, 300 W, pass energy = 200 eV, step size = 0.5 eV, 1 sweep. For high resolution scans the step size was 0.1 eV; 5 sweeps were carried out and averaged.

2.4. Modification procedure

Electrode grafting of the GC electrode with nitrophenyl groups was performed by cycling the potential three times between 0.4 and -0.4 V in a 10 mM solution of NBD in anhydrous acetonitrile containing 0.1 M $TBABF_4$ as base electrolyte at a sweep rate of 100 mV s^{-1}. A fixed potential of -0.25 V was applied for 300 s at the end of these cycles in order to ensure full surface coverage. The electrode was rinsed with acetonitrile and then sonicated in acetonitrile for 10 min. to remove excess NBD. It was then rinsed with acetone and water before use. The

attached $-NO_2$ groups were reduced first by cycling three times in 0.1 M aqueous KOH between 0 and -1.2 V and then holding the potential at -0.8 V for 300 s to ensure complete reduction of the attached nitrophenyl to nitrosophenyl groups. Gold deposition was carried out on this modified electrode by applying a potential step from 0.5 to –0.3 V for 0.5 s when in contact with a freshly prepared 1 mM solution of $HAuCl_4$ in 0.1 M KOH. The reason for using alkaline media was to provide a system (see below) that would display characteristic nucleation and growth phenomena that could be used to produce a nanoparticulate surface. The GC modified electrode was then rinsed thoroughly with water and cyclic voltammograms were recorded in Ar saturated solutions. The grafting and deposition procedures are outlined in Scheme 1.

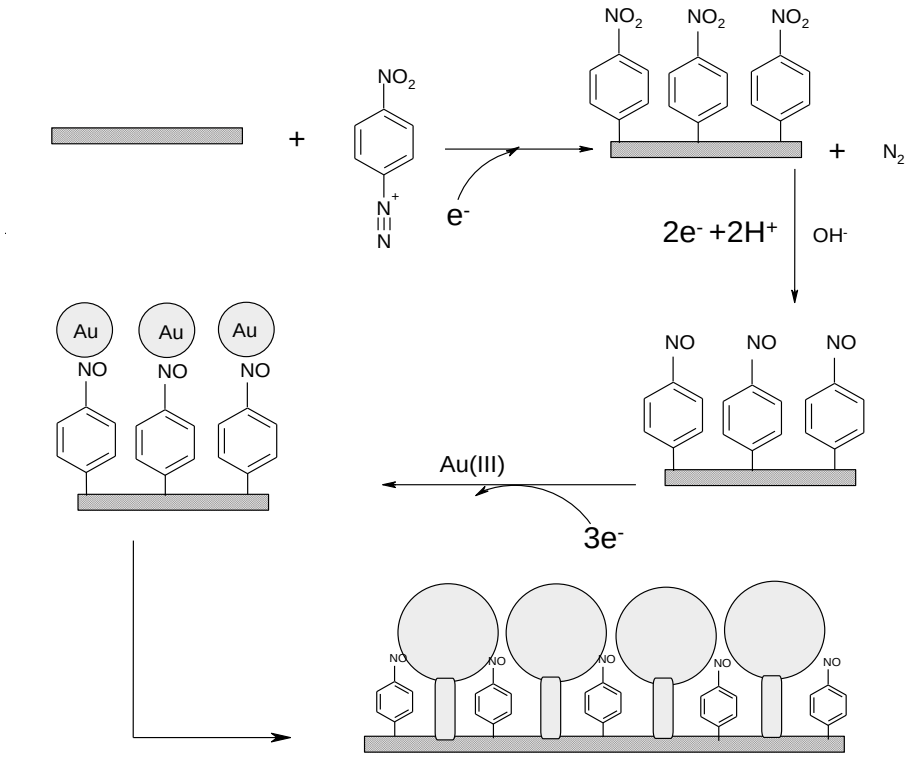

Scheme 1. Schematic description of the nucleation and growth of a nanostructured gold layer templated by a grafted film.

3. Results and discussion

3.1. Electrografting of the template molecular film

Figure 1 shows the cyclic voltammogram for the reductive grafting of NBD. A large irreversible cathodic wave is observed, which leads to the formation of the nitrophenyl radical and its attachment to the carbon surface. As previously observed, the current on the second sweep is greatly reduced due to coverage by nitrophenyl groups;[28-32] subsequent voltammetric scans show very low background currents (Figure 1).

3.2. Characterisation of the grafted organic film

3.2.1. XPS measurements

Figure 2 shows the XPS results for a functionalised electrode. The peaks for C, O and N in the survey spectrum clearly indicate the presence of the nitrophenyl film.[37] The high resolution spectrum in the N1s region (Figure 2) shows two peaks at 400 and 406 eV. These correspond to reduced forms of the nitro group (-NH_2 and/or –NHOH[38]) and to the NO_2 group, respectively.[38-40] The spectrum suggests that a partial reduction of the nitro groups might take place either during grafting or caused by the X-ray beam in the XPS chamber as observed for nitrobenzene grafted on carbon, various metals[38] and on SiO_2.[40]

3.2.2. Electrochemistry of the nitrophenyl film

The cyclic voltammetry of the grafted GC electrode in 0.1 M KOH is shown in Figure 3. A large reduction wave is observed at approximately -0.92 V in the first scan due to the irreversible reduction of the –NO_2 group followed by an oxidation peak at *ca* -0.43 V in the reverse cycle. Further reduction of the surface groups was not observed under these experimental conditions but in acid media, further irreversible reduction to the amine was observed at -1.1 V (data not shown).[38,39] The electrochemistry and electrocatalytic properties of the nitrophenyl monolayer film for the reduction of oxygen will be presented elsewhere.[41]

The surface groups present can be analysed from the known electrochemistry of nitrobenzene, which follows a two-step reduction in alkaline solutions.[38-39] The first step is a two-electron irreversible reduction to nitrosobenzene followed by a quasi-reversible two-electron, two-proton reduction to phenylhydroxylamine according to:[38-39]

$$Ar-NO_2 + 2H^+ + 2e^- \rightarrow Ar-N(OH)_2 \xrightarrow{-H_2O} Ar-NO + 2H^+ + 2e^- \rightleftharpoons Ar-NH(OH)$$

Scheme 2.

It is proposed that the reduction wave observed in the first cycle in Figure 3 corresponds to the formation of 4-nitrosophenyl groups (NOPh) according to Scheme 2. The voltammetric wave observed in subsequent scans corresponds to the reduction of the nitroso group as previously observed for the reduction of nitrosobenzene.[38] The surface coverage of the modified electrode was calculated from the average charge density under the voltammetric peaks at various sweep rates according to $\Gamma=Q/nFA$, where Q is the charge under the peak, n is the number of electrons involved, F is the Faraday constant and A is the electrode area.[33] A surface concentration of $(9\pm3)\times10^{-10}$ mol cm^{-2} was found considering n=2 (Scheme 2). The surface coverage for a monolayer of 4-nitrophenyl groups calculated from its molecular dimensions is 1.25×10^{-9} mol cm^{-2}.[29] Therefore, the film obtained from the grafting procedure has a coverage less than or close to a compact monolayer. Thus, the reduction of the surface nitrophenyl groups leads to electron-rich 4-nitrosophenyl substituents (NOPh) which can provide nucleation centres for the electrodeposition of gold and the whole film can then act as a template for the confined growth of a nanostructured metal electrodeposit. This is the idea that was explored in what follows.

3.3. Electrodeposition of gold on a NOPh grafted GC electrode

Alkaline $AuCl_4^-$ solutions were used for the electrodeposition of gold since these appeared to provide a better medium for nucleation and growth of nanocrystals than those from neutral or acidic solutions. $AuCl_4^-$ decomposes slowly in 0.1 M KOH with a half-life time for the full decomposition of several hours[42] forming soluble intermediate hydroxychloro gold(III) $[Au(OH)_xCl_{4-x}]^-$ complexes.[43] The final product is the soluble form of the weakly acidic $Au(OH)_3$. The equilibrium solubility of gold hydroxide at room temperature in 0.1 M NaOH is 0.1 mM.[44] A concentration of $AuCl_4^-$ in 0.1 M KOH higher than this was employed in the present work but the solutions were freshly prepared before use and no precipitation of $Au(OH)_3$ was observed, as also reported by others.[45]

Figure 4 compares the first scan for the deposition voltammograms of Au(III) on bare GC and GC grafted with 4-nitrosophenyl groups (GC/NOPh). Electrodeposition on both surfaces shows a characteristic nucleation and growth current-potential feature, with a sharp maximum in the current during the nucleation step followed by the characteristic growth features changing form spherical to linear diffusion. The current crossover observed for the forward and reverse scans is due to the growth of gold on the centres formed during the nucleation step. The crossover potential has been used as an estimate of the formal potential of the metal couple[12,46] and values of 0.16 and 0.24 V were observed for deposits on GC and on the template film. The nucleation and growth potentials were approximately 0.06±0.02 V for bare GC and 0.19±0.02 V for NOPh grafted GC. These potentials are much more negative than those previously reported for gold deposition on a boron-doped diamond electrode in 0.1 M H_2SO_4 (0.67 V).[12] The difference is due to the formation of chloro-hydroxo complexes of gold in the alkaline medium. The gold functionalised electrode (GC/NOPh(Au)) was prepared as described in Section 2.4.

Coordination of a metal ion shifts its deposition potential to more negative values.[21-23] However, the positive potential shift observed between bare and templated glassy carbon is probably due to the strong interaction of the nitroso groups present on the template film with the electrodeposited gold. Weaver *et al* demonstrated that nitrosobenzene is strongly adsorbed on gold in alkaline media but not in acid solutions using Surface Enhanced Raman Spectroscopy (SERS).[47] In consequence, a positive shift of the nucleation and deposition potential of small metal clusters due to their interaction with the template medium would be expected. The deposition current observed for the NOPh modified GC is greater than that of bare GC for similar experimental conditions (Figure 4) after differences in concentrations are factored in, indicating a higher number of nucleation sites for the former.

Figure 5 shows that the functionalisation of GC provides a template for the nucleation of a nanostructured film. Figure 5a shows an AFM image of the Au deposit on GC/NOPh. Individual nanosized islands of gold with average size of 20-25 nm are observed. Figure 5b shows a typical cyclic voltammogram of this modified electrode in 0.1 M H_2SO_4. The

oxidation and reduction waves for this surface are similar to those observed for bulk gold.[23] The charge under the cathodic wave was approximately 940 μC cm^{-2}. The charge required to form an oxide monolayer on gold[48] is 400 μC cm^{-2} and hence the roughness factor of the modified electrode was approximately 2.4. Similar voltammograms in an acid solution have been reported for Au nanoparticles chemically attached to surfaces through bifunctional linkers,[49] for thin Au films deposited by vacuum evaporation [50,51] and for gold nanoparticles attached to multi-walled carbon nanotubes.[52]

The presence of metallic gold was demonstrated by XPS. The high resolution spectrum in the Au 4f region (Figure 6) shows the Au $4f_{7/2}$ and $4f_{5/2}$ peaks at 83.8 and 87.6 eV of metallic gold, in agreement with literature values of 84.0 and 87.7 eV.[53]

3.4. O_2 reduction on GC/NOPh(Au) electrodes

3.4.1. Acid solutions

Figure 7 shows the reduction of O_2 on a GC/NOPh(Au) electrode in 0.1 M H_2SO_4 and the corresponding potential dependence of *n* obtained by fitting the experimental results to Equation (1). *n* has a value of three at low potentials increasing to four as the potential is made more negative. These measurements were limited to $E > -0.45$ V due to the onset of hydrogen evolution. The increasing contribution of the $4e^-$ pathway with increasing negative potentials is similar to previous results obtained with thermally deposited thin Au films on GC[50,51] but different from those obtained by El-Deab and Ohsaka who compared O_2 reduction on electrodeposited gold nanoparticles with bulk gold.[14] A value of $n=4$ was found for the former and 3 for bulk Au[14] indicating that nanostructured gold is more reactive towards further reduction and/or disproportionation of peroxide.[27] The electroreduction of H_2O_2 starts at ca. -0.15 V (SCE) and therefore, further reduction of the peroxide formed takes place simultaneously with O_2 reduction.[54] These results highlight the profound influence of geometry of the electrodeposited metal on reduction kinetics.

3.4.2. Alkaline solutions

Figure 8 compares cyclic voltammograms of a GC electrode in Ar saturated 0.1 M KOH before and after modification with NOPh and after Au deposition. After functionalisation, the characteristic redox processes for the Ar-NO/Ar-NHOH couple are observed (See also Figure 3). After Au deposition, the voltammogram for the GC/NOPh electrode is extensively suppressed, a consequence of the strong interaction between the nitroso groups and the deposited gold, as previously described by Weaver *et al*.[47] In the presence of oxygen, the reduction of O_2 on the GC/NOPh electrode is partially inhibited by the attached film but the inclusion of Au within the film results in the appearance of two well-defined voltammetric waves indicating that the electrodeposited Au provides electrical communication with the substrate.

The presence of two reduction waves was further investigated using a rotating disk electrode. Figure 9 compares the reduction of O_2 at a rotating GC disk electrode with various surface modifications. The lower limiting reduction current observed compared with bulk gold (Figure 9a) is due to partial blocking of the GC active surface by the attached nitrosophenyl film. In addition, no large catalytic wave associated with the reduction of Ar-NO or with its reduced form is observed showing that the reduced substrate has a low reactivity towards oxygen. In contrast with bulk gold, the disk and ring currents clearly indicate a two-step reduction for the GC/NOPh(Au) electrode. The amount of peroxide produced on the GC/NOPh(Au) electrode reaches a maximum at approximately -0.7 V and then decreases at more negative potentials. This is not the case for unmodified GC or GC/NOPh electrodes for which the production of peroxide increases for $E < -0.7$ V. Figure 9 also clearly shows that the two-step reduction is a property of the Au deposited on the template film and not of the underlying GC surface or the NOPh film. The typical bell-shaped ring currents (Figure 9b) is a clear indication of peroxide formation and its further reduction at more negative potentials.[55]

Figure 10 shows the RDE polarisation curves for O_2 reduction on the GC/NOPh(Au) electrode at several rotation rates. Although the ring currents clearly demonstrated the formation of peroxide these had a poor reproducibility and were not quantitative, probably due to contamination by attached and/or adsorbed nitro- or nitrosobenzene and therefore, the RRDE mechanistic diagnostic criteria[56] could not be applied. These results show the presence of two

distinguishable reaction mechanisms, a $2e^-$ reduction at potentials more positive than -0.9 V and a $4e^-$ reduction at more negative potentials, in accordance with the cyclic voltammetry results (Figure 8). To the authors' knowledge, this is the first report of a well-defined two-step oxygen reduction on a gold nanoparticulate surface. Previous work by Ohsaka *et al.*[57] demonstrated two overlapping waves corresponding to the $2e^-$ and the $4e^-$ reactions in 0.1 M phosphate buffer (pH=7.2) for Au electrodeposited on GC. The efficiency of H_2O_2 production was dependent on Au loading and the two-step reduction was only observed for very small Au loadings *i.e.*, for small particle sizes.[57] The trend observed in the present work in alkaline media highlights the influence of metal deposition conditions on product distribution and hence, of the surface structures obtained. The contributions of the GC electrode support to the measured currents are minimal and both the grafted nitrophenyl film and the gold layer effectively block the substrate.

The potential dependence of *n* is shown in Figure 11 where it can be seen that the calculated values of *n* are close to two and four for the first and second reduction steps, respectively. These results are confirmed qualitatively by the ring currents shown in Figure 9b. This behaviour is very different from that observed for bulk gold[57] indicating that the nanostructured Au surface induces significant changes in the reduction mechanism.

The sensitivity of the kinetics of oxygen reduction to surface structure has been known for a long time.[58-63] The effect of crystalline orientation has been extensively analysed by Štrbac and Adžić.[63] These authors demonstrated that the reduction mechanism is determined by the chemisorptions of the OH^- ion to yield $AuOH^{(1-\lambda)-}$. The (100) orientation supports the $4e^-$ reduction while the (111) and (332) surfaces lead almost exclusively to peroxide in the whole potential range. The details of these reactions are unclear but recent studies by Kim and Gewirth using surface enhanced Raman spectroscopy (SERS) and density functional theory calculations (DFT)[27] indicate that decomposition of the peroxide produced is catalyzed by the adsorbed OH species but only on the Au(100) surface. Thus, the four-electron reduction of oxygen on Au(100) in basic media is accomplished by the disproportionation of peroxide resulting from the first two-electron transfer steps.[27] A change in reaction pathway from $2e^-$ to $4e^-$ at more negative potentials was observed and ascribed to the potential dependence of the

hydroxide adsorption on Au(100) that catalyzes the reduction of peroxide.[62] This change of coverage by adsorbed -OH species leads to a current maximum which is also observed for polycrystalline Au in 0.1 M KOH (see Figure 9) but not for the GC/NOPh(Au) electrode (Figure 10). A similar trend was also observed by Kuzume *et al*. for a Au surface modified with adsorbed fullerene.[64] Fullerene is inactive for O_2 reduction and its adsorption on Au alters the adsorption sites for the first reduction intermediate due to a surface blocking effect.

The behaviour observed does not correspond to the underlying NOPh film or to the GC electrode support due to the blockage of the GC surface by the attached film. Štrbac and Adžić have commented[63] that for all the crystal orientations studied that lead to the reduction to water at sufficiently negative potentials, a single reduction wave is not observed, *i.e.* the activation energies for the $2e^-$ and $4e^-$ channels are not very different. Not much information on the electrochemical properties of well-defined gold nanoparticles is available since only recently attempts have been made to relate their surface structure to their reactivity.[65-68] Oxygen reduction on gold is a strongly surface sensitive reaction. Hernández *et al*.[66] showed that Au nanoparticles and nanorods containing only (111) or (110) and no (100) surfaces catalyse the two-electron reduction. In addition, 40 nm Au nanoparticles of preferentially cubic shape suggesting high percentage of Au(100) domains catalysed the $4e^-$ reduction of O_2 in alkaline solution.[67] These results correlate well with single crystal studies.

The present results are comparable to those obtained from 30 or 40 nm Au films vacuum evaporated on pyrolytic graphite[68] suggesting a similar crystalline ordering to that for films on a this support. Similar morphological dependence of electrocatalytic activity of nanoparticulate gold was observed by Jena and Raj who noted two well-defined voltammetric waves for ascorbate oxidation, different from that of bulk gold.[69] The results in Figure 11 do not show a distinction between the different crystal orientation and the surfaces studied here have very different properties from those of single crystals or indeed, of polycrystalline Au. The difference between these electrodes and polycrystalline surfaces is the size of the domains. For surfaces modified with adsorbed fullerene it is known that a decrease in the domain size leads to a $2e^-$ reduction mechanism.[64] The size of the domains of the surfaces studied (Figure 5a) is, however, too large to account for the influence of orientation changes of adsorbed O_2 proposed

in Ref. 64. A possible explanation for the unusual results in Figure 11 could be surface restructuring as the potential is made more negative, thus changing surface morphology. Detailed structural studies are required, however, for a full understanding of these unusual effects.

3.4.3 The EE reduction mechanism

The results in Figure 10 are further analyzed considering a simple two-step, two-electron transfer sequential reaction (the EE mechanism):[55]

$$O_2 + H_2O + 2e^- \rightarrow HO_2^- + OH^- \qquad \text{(I)}$$

$$HO_2^- + H_2O + 2e^- \rightarrow 3OH^- \qquad \text{(II)}$$

The two reaction steps are taken as irreversible and to follow a simple electron transfer rate determining step.[35] The dependence of the current density on potential at different rotation rates for an EE mechanism is given by:[55]

$$j^{-1} = \left[j_D^{-1} - \frac{1}{2Fc_{o_2}^b k_I^{0'} \exp(-\alpha_I f(E - E_I^0))} \right] \left[\frac{2Fc_{o_2}^b k_{II}^{0'} \exp(-\alpha_{II} f(E - E_{II}^0)) - j_D}{4Fc_{o_2}^b k_{II}^{0'} \exp(-\alpha_{II} f(E - E_{II}^0)) - j_D} \right] \qquad (2)$$

where j is the current density at potential E, j_D is the limiting current density for the first reduction step (Reaction (I)), F is the Faraday constant, $c_{o_2}^b$ is the bulk concentration of oxygen, k_I^0' and k_{II}^0' are the electrochemical rate constants and E_I^0 and E_{II}^0 are the standard potentials for Reactions (I) and (II), respectively, α_I and α_{II} are the corresponding transfer coefficients and $f = F/RT$. For the calculations of the rate constants, the potentials were referred to the same standard potential, that of Reaction (I), in order to be able to compare the Gibbs energy of activation for the two consecutive reactions. Thus, in the non-linear regression, E_{II}^0 was set equal to E_I^0, at -0.315 V.

Equation (2) can be obtained from the general case presented by Sakai and Ohnaka[55] by setting Λ_{12} and Λ_{22} to zero in Equations (7), (8) and (9) of Ref. 55 for the irreversible case discussed here and using the convention that cathodic currents are negative. A simple derivation of Equation (2) is also given as Supporting Information. The results shown in Figure 11 were fitted to Equation (2) by non-linear regression.[70] In order to avoid uncertainties with the regression analysis, the charge transfer coefficients were not considered as variables, thus reducing the number of independent variables to be fitted. α_1 and α_2 were estimated from the potential dependence of the current function $\log(-j \times j_D/(j_D-j))$ in the potential regions for which $n<2$ and $2<n<4$. Average values of $\alpha_1 = 0.3$ and $\alpha_2 = 0.6$ were obtained. These values were kept constant during the regression analysis. A comparison of experimental and calculated currents is shown in Figure 11 where it can be seen that a reasonably good fit is obtained. The rate constants calculated from this analysis for all the rotation rates studied were $k_I^{0'} = (1.5 \pm 0.1) \times 10^{-3}$ cm s^{-1} and $k_{II}^{0'} = (2.2 \pm 0.2) \times 10^{-9}$ cm s^{-1}. For the reasons discussed above, the latter value was calculated at the standard potential of Reaction (I). Although the above is an oversimplified reaction model (e.g., no intermediate chemical steps are considered), it is significant that it reproduces well the experimental current-potential curves. The values of the rate constants correspond to a difference in Gibbs energy of activation between the first and second step of approximately 33 kJ mol^{-1}.

4. Conclusions

A NOPh grafted GC electrode provides a good substrate for the electrodeposition of Au nanostructures in alkaline solution for the study of the reduction of O_2. An electrochemically reduced nitrophenyl film provided a suitable template for the adsorption of gold complexes followed by controlled electrodeposition to produce a nanostructured Au surface. Gold electrodeposition is facilitated by the presence of reduced nitrophenyl groups. The electrocatalytic properties of these surfaces are very different from those of the bulk metal both in acid and alkaline solutions. A clear distinction between the $2e^-$ and the $4e^-$ reduction pathways is observed for the latter and it is shown that the modified electrode partially inhibits the $4e^-$ O_2 reduction pathway compared with bulk Au electrodes. The potential dependence of the current could be fitted to an EE mechanism and the difference in Gibbs energy of activation

between the $2e^-$ and the $4e^-$ pathways was 33 kJ mol^{-1}. The nanostructured surfaces prepared appear promising for the selective reduction of oxygen to hydrogen peroxide in alkaline solutions.

Acknowledgements

The support from the European Union, NENA project, FP6 programme, is gratefully acknowledged. This research was partly supported by the Estonian Science Foundation (Grant No. 7546). We would also like to thank Dr. Leonard Matisen and Dr. Agu Saar (Institute of Physics, University of Tartu) for their help in XPS measurements.

References

1. A. Wieckowski, E. Savinova and C. G. Vayenas, *Catalysis and Electrocatalysis at Nanoparticle Surfaces*, Marcel Dekker, New York, 2003.
2. J. H. Fendler, *Nanoparticles and Nanostructured Films*, Wiley-VCH, Weinheim, 1998.
3. R. Narayanan and M. A. El-Sayed, *J. Phys. Chem. B.*, 2005, **109**, 12663.
4. M. S. El-Deab, T. Sotomura and T. Ohsaka, *Electrochem. Commun*., 2005, **7**, 29.
5. Y. Shen, J. Liu, A. Wu, J. Jiang, L. Bi, B. Liu, Z. Li and S. Dong, *Langmuir*, 2003, **19**, 5397.
6. M. M. Waje, X. Wang, W. Li and Y. Yan, *Nanotechnology*, 2005, **16**, *S395*.
7. Y. Jin, Y. Shen and S. Dong, *J. Phys. Chem. B*, 2004, **108**, 8142.
8. M. Bayati, J. M. Abad, C. A. Bridges, M. J. Rosseinsky and D. J. Schiffrin, *J. Electroanal. Chem.*, 2008, **623**, 19.
9. D.-J. Guo and H.-L. Li, *Electroanalysis*, 2005, **17**, 869.
10. D.-J. Guo and H.-L. Li, *Carbon*, 2005, **43**, 1259.
11. D.-J. Guo and H.-L. Li, *Electrochem. Commun*., 2004, **6**, 999.
12. Y. Zhang, S.Asahina, S. Yoshihara and T. Shirakashi, *Electrochim. Acta*, 2003, **48**, 741.
13. K. B. Holt, G. Sabin, R. G. Compton, J. S. Foord and F. Marken, *Electroanalysis*, 2002, **14**, 797.
14. M. S. El-Deab and T. Ohsaka, *Electrochim. Acta*, 2002, **47**, 4255.
15. M. S. El-Deab and T. Ohsaka, *J. Electroanal. Chem.*, 2003, **553**, 107.
16. M. O. Finot, G. D. Braybrook and M. T. McDermott, *J. Electroanal. Chem.*, 1999**, 466**, 234.
17. C. D. Keating and M. J. Natan, *Adv. Mater.*, 2003, **15**, 451.
18. L. A. Baker, P. Jin and C. R. Martin, *Crit. Rev. Solid State Mater. Sci.*, 2005**, 30**, 183.
19. C. A. Foss, G. L. Hornyak, J. A. Stockert and C. R. Martin, *J. Phys. Chem.*, 1994, **98**, 2963.
20. S.-J. Choi, D.-H. Woo, N. Myung, H. Kong and S.-M. Park, *J. Electrochem. Soc.*, 2001, **148**, C569.
21. V. Ivanova, T. Baunach and D. M. Kolb, *Electrochim. Acta*, 2005, **50**, 4283.
22. M. Manolova, V. Ivanova, D. M. Kolb, H.-G. Boyen, P. Ziemann, M. Büttner, A. Romanyuk and P. Oelhafen, *Surf. Sci.*, 2005, **590**, 146.
23. Y.-C. Yang, S.-L. Yau and Y.-L. Lee, *J. Am. Chem. Soc.*, 2006, **128**, 3677.
24. R. Adžić, in *Electrocatalysis*, ed. J. Lipkowski and P. N. Ross, Wiley-VCH, New York, 1998, pp. 197-242.
25. E. Yeager, *Electrochim. Acta*, 1984, **29**, 1527.
26. A. Damjanovic, M. A. Genshaw and J. O'M. Bockris, *J. Electroanal. Chem.*, 1967, **15**, 173.
27. J. Kim and A. A. Gewirth, *J. Phys. Chem. B*, 2006, **110**, 2565.
28. M. Delamar, R. Hitmi, J. Pinson and J. M. Savéant, *J. Am. Chem. Soc.*, 1992, **114**, 5883.

29. P. Allongue, M. Delamar, B. Desbat, O. Fagebaume, R. Hitmi, J. Pinson and J.-M. Saveant, *J. Am. Chem. Soc.*, 1997, **119**, 201.
30. M. P. Stewart, F. Maya, D. V. Kosynkin, S. M. Dirk, J. J. Stapleton, C. L. McGuiness, D. L. Allara and J. M. Tour, *J. Am. Chem. Soc.*, 2004, **126**, 370.
31. J. Pinson and F. Podvorica, *Chem. Soc. Rev*., 2005, **34**, 429.
32. A. Laforgue, T. Addou and D. Bélanger, *Langmuir*, 2005, **21**, 6855.
33. A. J. Bard and L. R. Faulkner, *Electrochemical Methods: Fundamentals and Applications*, Wiley, New York, 1980.
34. E. Ahlberg, F. Falkenberg, J. A. Manzanares and D. J. Schiffrin, *J. Electroanal. Chem*., 2003, **548**, 85.
35. R. E. Davis, G. L. Horvath and C. W. Tobias, *Electrochim. Acta*, 1967, **12**, 287.
36. D. R. Lide, (ed.); *CRC Handbook of Chemistry and Physics*, 82nd edn., CRC Press, Boca Raton, 2001.
37. Y.-C. Liu and R. L. McCreery, *J. Am. Chem. Soc.*, 1995, **117**, 11254.
38. H. Tsutsumi, S. Furumoto, M. Morita and Y. Matsuda, *J. Coll. Int. Sci.*, 1995, **171**, 505; B. Ortiz, C. Saby, G. Y. Champagne and D. Bélanger, *J. Electroanal. Chem.*, 1998, **455**, 75; P. Zuman and Z. Fijalek, *J. Electroanal. Chem.* 1990, **296**, 589; L.-J. Fan, C. Wang, S.-C. Chang and Y.-W. Yang, *J. Electroanal. Chem.*, 1999, **477**, 111; P. A. Brooksby and A. J. Downard, *Langmuir*, 2004, **12**, 5038.
39. A. Adenier, E. Cabet-Deliry, A. Chaussé, S. Griveau, F. Mercier, J. Pinson and C.Vautrin-Ul, *Chem. Mater*., 2005, **17**, 491.
40. P. Mendes, M. Belloni, M. Ashworth, C. Hardly, K. Nikitin, D. Fitzmaurice, K. Critchley, S. Evans and J. Preece, *ChemPhysChem*, 2003, **4**, 884.
41. F. Mirkhalaf and D. J. Schiffrin, *Manuscript in Preparation*.
42. Determined from UV-vis spectroscopy (results not shown).
43. F. A. Cotton and G. Wilkinson, *Advanced Inorganic Chemistry*, 3rd edn., J. Wiley Interscience, 1972, p. 1052; S. Ivanova, C. Petit and V. Pitchon, *Appl. Catal. A*, 2004, **267**, 191.
44. H. L. Johnston and H. L. Leland, *J. Am. Chem. Soc.*, 1938, **60**, 1439.
45. A. Corma and H. Garcia, *Chem. Soc. Rev*., 2008, **37**, 2096.
46. U. Schmidt, M. Donten and J. G. Osteryoung, *J. Electrochem. Soc.*, 1997**, 144**, 2013; G. Trejo, A. F. Gil and L. González, *J. Electrochem. Soc.*, 1995, **142**, 3404; K. Márquez, R. Ortiz, J. W. Schultze O. P. Márquez, J. Márquez and G. Staikov, *Electrochim. Acta*, 2003, **48**, 711; P. C. T. D'Ajello and A. Q. Schervenski, *J. Electroanal. Chem.*, 2004, **573**, 37.
47. P. Gao, D. Gosztola and M. J. Weaver, *J. Phys. Chem.*, 1988, **92**, 7122.

48. H. Angerstein-Kozlowska, in: *Comprehensive Treatise of Electrochemistry*, ed. E. Yeager, J. O'M. Bockris, B. E. Conway and S. Sarangapani, Plenum Press, New York, 1984, Vol. 9, pp. 15-59.
49. J. Lee, S. Hwang, H. Lee and J. Kwak, *J. Phys. Chem. B*, 2004**, 108**, 5372.
50. A. Sarapuu, K. Tammeveski, T. T. Tenno, V. Sammelselg, K. Kontturi and D. J. Schiffrin, *Electrochem. Commun.*, 2001**, 3**, 446.
51. A. Sarapuu, M. Nurmik, H. Mändar, A. Rosental, T. Laaksonen, K. Kontturi, D. J. Schiffrin and K. Tammeveski, *J. Electroanal. Chem.*, 2008, **612**, 78.
52. N. Alexeyeva, K. Kontturi, T. Laaksonen, F. Mirkhalaf, D. J. Schiffrin and K. Tammeveski, *Electrochem. Commun.*, 2006, **8**, 1475
53. K. Takahiro, S. Oizumi, A. Terai, K. Kawatsura, B. Tsuchiya, S. Nagata, S. Yamamoto, H. Naramoto, K. Narumi and M. Sasase, *J. Appl. Phys.*, 2006**, 100**, 084325.
54. R. Zeis, T. Lei, K. Siera, J. Snyder, and J. Erlebacher, *J. Catalysis*, 2008, **253**, 132.
55. M. Sakai and N. Ohnaka, *J. Electrochem. Soc.*, 1990, **137**, 576.
56. H. S. Wroblowa, Y.-C. Pan and G. Razumney, *J. Electroanal. Chem.*, 1976, **69**, 195.
57. M. S. El-Deab, T. Okajima and T. Ohsaka, *J. Electrochem. Soc.*, 2003**, 150**, A851.
58. R. R. Adžić, N. M. Marković and V. B. Vešović, *J. Electroanal. Chem.*, 1984, **165**, 105.
59. N. M. Marković, R. R. Adžić and V. B. Vešović, *J. Electroanal. Chem.*, 1984, **165**, 121.
60. S. Štrbac, N. A. Anatasijević and R. R. Adžić, *J. Electroanal. Chem.*, 1992**, 323**, 179.
61. A. Prieto, J. Hernández, E. Herrero and J. M. Feliu, *J. Solid State Electrochem.*, 2003, **7**, 599.
62. N. M. Markovic, I. M. Tidswell and P. N. Ross, *Langmuir*, 1994, **10**, 1.
63. S. Štrbac and R. R. Adžić, *J. Electroanal. Chem.*, 1996, **403**, 169.
64. A. Kuzume, E. Herrero, J. Feliu, E. Ahlberg, R. J. Nichols and D. J. Schiffrin, *Phys. Chem. Chem. Phys.*, 2005, **7**, 1293.
65. J. Hernández, J. Solla-Gullón, E. Herrero, *J. Electroanal. Chem.*, 2004, **574**, 185.
66. J. Hernández, J. Solla-Gullón, E. Herrero, A. Aldaz and J. M. Feliu, *J. Phys. Chem. B*, 2005, **109**, 12651.
67. J. Hernández, J. Solla-Gullón, E. Herrero, A. Aldaz and J. M. Feliu, *J. Phys. Chem. C*, 2007, **111**, 14078.
68. C. Paliterio, A. Hamnett and J. B. Goodenough, *J. Electroanal. Chem.*, 1987, **234**, 193.
69. B. K. Jena and C. R. Raj, *Electrochem. Commun.*, 2008, **10**, 951.
70. K. Tammeveski, K. Kontturi, R. J. Nichols, R. J. Potter and D. J. Schiffrin, *J. Electroanal. Chem.*, 2001, **515**, 101; A. Sarapuu, K. Vaik, D. J. Schiffrin and K. Tammeveski, *J. Electroanal. Chem.*, 2003, **541**, 23; K. Vaik, A. Sarapuu, K. Tammeveski, F. Mirkhalaf and D. J. Schiffrin, *J.*

Electroanal. Chem., 2004, **564**, 159; F. Mirkhalaf, K.Tammeveski and D. J. Schiffrin, *Phys. Chem. Chem. Phys*., 2004, **6**, 1321; M. Kullapere, G. Jürmann, T. T. Tenno, J. J. Paprotny, F. Mirkhalaf and K. Tammeveski, *J. Electroanal. Chem.*, 2007, **599**, 183; G. Jürmann, D. J. Schiffrin and K. Tammeveski, *Electrochim. Acta*, 2007, **53**, 390; J.-M. Seinberg, M. Kullapere, U. Mäeorg, F. C. Maschion, G. Maia, D. J. Schiffrin and K. Tammeveski, *J. Electroanal. Chem*., 2008,**624, 151**; M. Kullapere, J.-M. Seinberg, U. Mäeorg, G. Maia, D. J. Schiffrin and K. Tammeveski, *Electrochim. Acta*, 2008, doi:10.1016/j.electacta.2008.08.054.

Legends to Figures

Figure 1. Electrografting scans of 10 mM 4-nitrobenzenediazonium tetrafluoroborate in acetonitrile for the first (solid line), second (dotted line) and third (dashed line) cycles. Sweep rate=100 mV s^{-1}; base electrolyte = 0.1 M tetrabutylammonium tetrafluoroborate.

Figure 2. XPS survey spectra and high-resolution XPS spectra of the N1s region for the nitrophenyl modified glassy carbon electrode.

Figure 3. Cyclic voltammograms for a nitrophenyl-modified GC electrode in 0.1 M KOH; (1) first scan (dashed line) and (2) second scan (solid line). Sweep rate = 20 mV s^{-1}.

Figure 4. First scan cyclic voltammograms for the electrodeposition of gold on NOPh functionalised GC (solid curve) and bare GC (dotted curve) from 1 mM and 0.45 mM $HAuCl_4$ in 0.1 M KOH, respectively, and for a bare GC (dashed curve) in 0.1 M KOH solution. Sweep rate= 20 mV s^{-1}.

Figure 5. a) AFM image of a GC electrode after surface derivatisation and Au deposition; b) Cyclic voltammogram of a GC/NOPh (Au) electrode in Ar saturated 0.1 M H_2SO_4. Sweep rate=20 mV s^{-1}.

Figure 6. XPS spectrum of the Au4f region for a GC/NOPh (Au) electrode.

Figure 7. Current-potential curves for oxygen reduction on a GC/NOPh(Au) electrode in O_2 saturated 0.1 M H_2SO_4. Rotation rates: 200, 400, 800, 1500, 2500, and 3500 rpm. The inset shows the potential dependence of *n* calculated from the K-L plots.

Figure 8. Cyclic voltammograms of bare GC, GC/NOPh and GC/NOPh(Au) electrodes in Ar saturated 0.1 M KOH and GC/NOPh and GC/NOPh(Au) in O_2 saturated 0.1 M KOH solution. Sweep rate= 20 mV s^{-1}.

Figure 9. Comparison of O_2 reduction on bare GC and Au with that of the modified GC electrodes at a rotation rate of 400 rpm in 0.1 M KOH; (a) disk and (b) ring currents.

Figure 10. O_2 reduction on a GC/NOPh(Au) electrode in O_2 saturated 0.1 M KOH. Rotation rates: (1) 200, (2) 400, (3) 800, (4) 1500, (5) 2500, (6) 3500 rpm.

Figure 11. Example of a non-linear regression simulation curve fit for a RDE oxygen reduction voltammogram from Fig. 10 at a rotation rate of 800 rpm. The parameters used are described in the text. The inset is the potential dependence of *n* for the reduction of O_2 on a GC/NOPh(Au) electrode in 0.1 M KOH calculated from the Koutecky-Levich plots of the data in Figure 10.

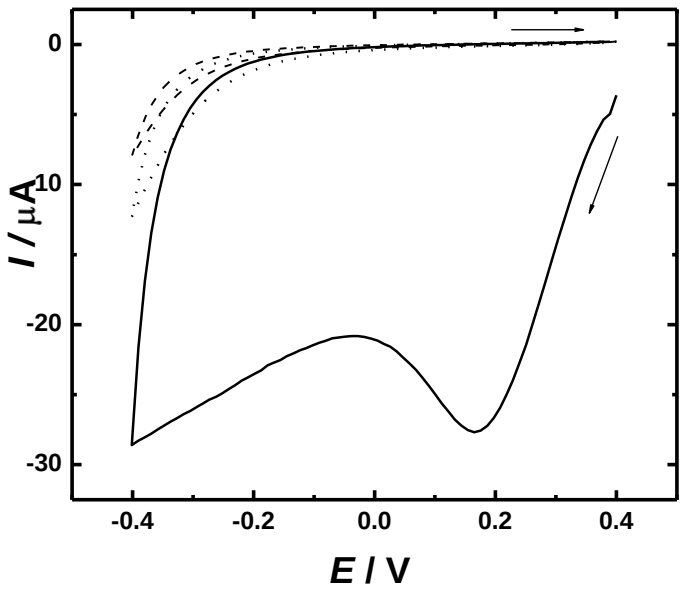
0
-10
-20
-30
I / μA
-0.4
-0.2
0.0
0.2
0.4
E / V

Fig. 1.

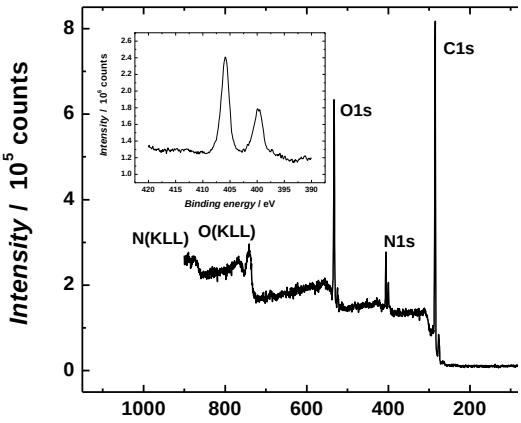
Intensity / 10^5 counts
8
6
4
2
0
1000
800
600
400
200
C1s
O1s
N1s
N(KLL)
O(KLL)
Binding energy / eV

Fig. 2.

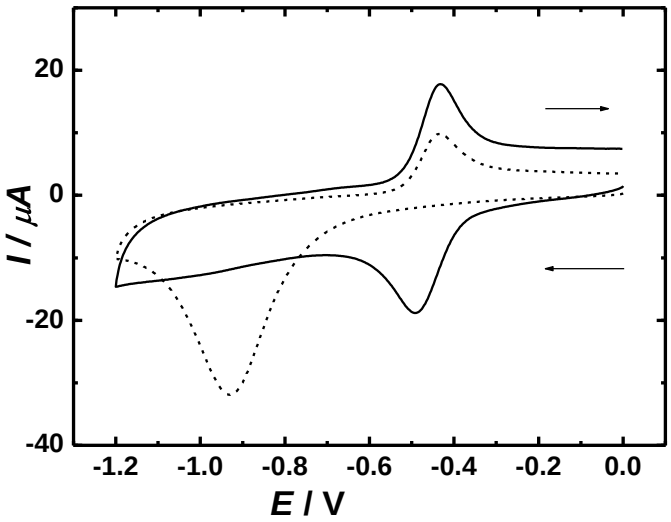

Fig. 3.

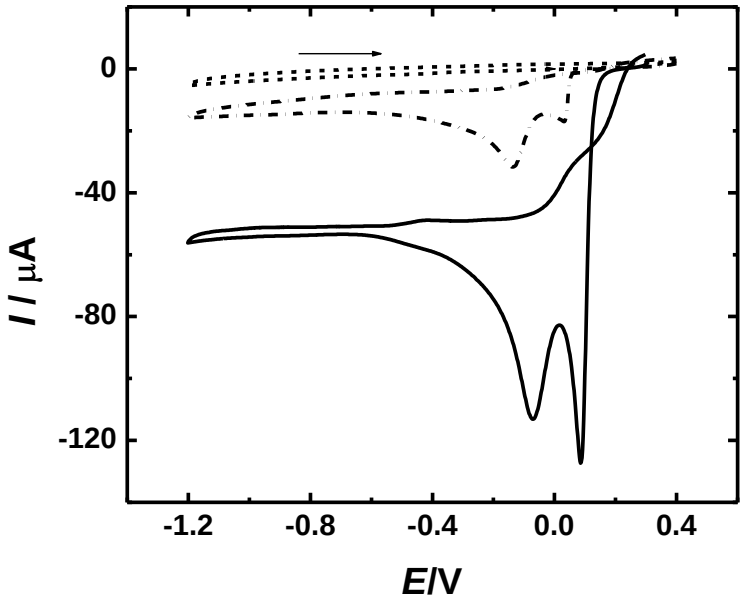

Fig. 4.

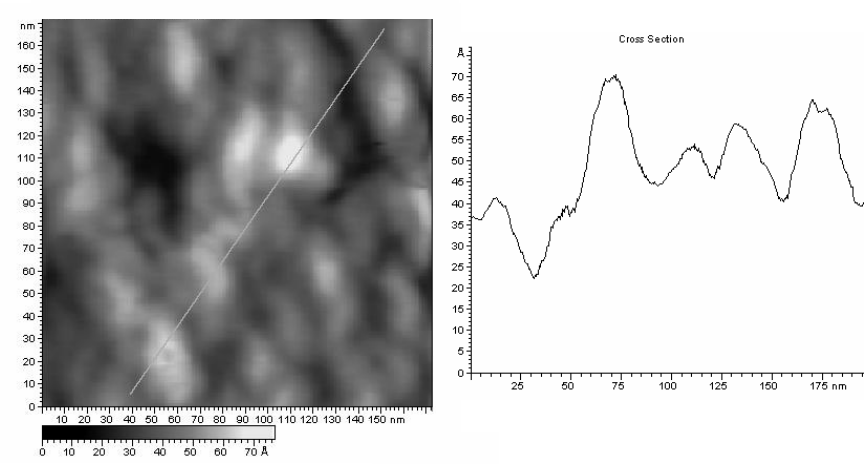
Cross Section
nm
Å
10 20 30 40 50 60 70 80 90 100 110 120 130 140 150 nm
0 10 20 30 40 50 60 70 Å
25 50 75 100 125 150 175 nm

(a)

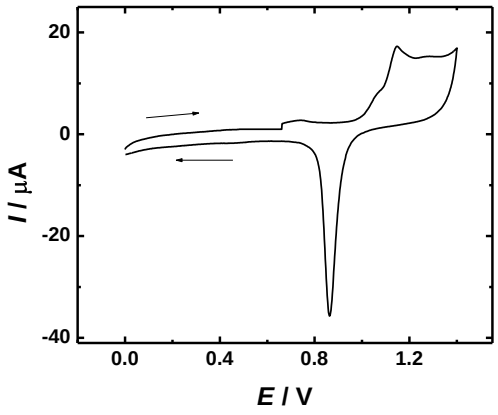
20
0
-20
-40
0.0
0.4
0.8
1.2
I / µA
E / V

(b)

Fig. 5.

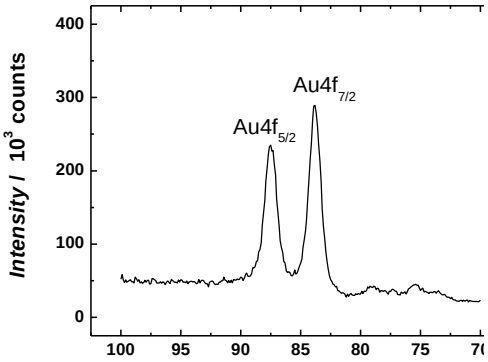

Figure 6

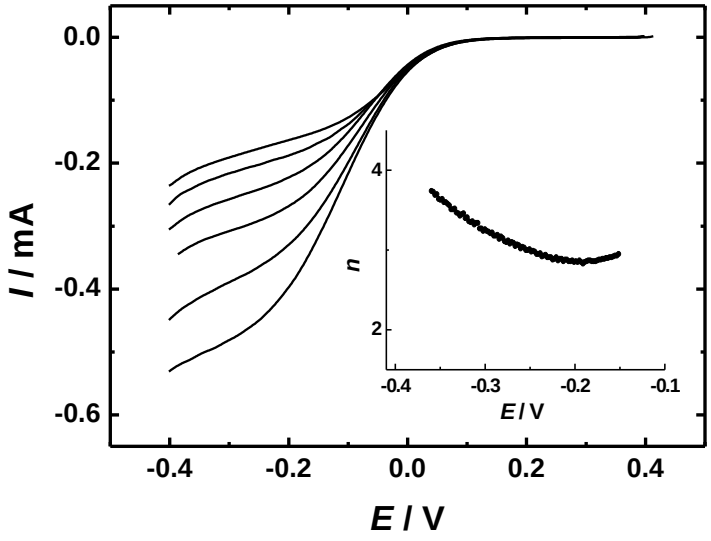

Fig. 7.

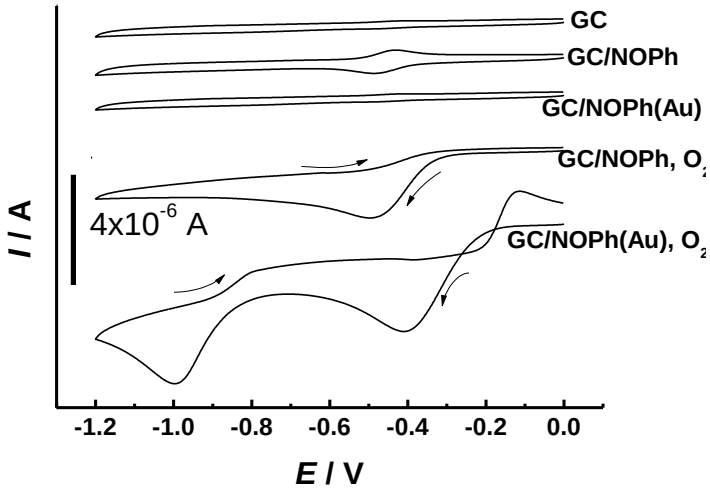
GC
GC/NOPh
GC/NOPh(Au)
GC/NOPh, O2
4x10-6 A
GC/NOPh(Au), O2
I / A
-1.2
-1.0
-0.8
-0.6
-0.4
-0.2
0.0
E / V

Fig. 8.

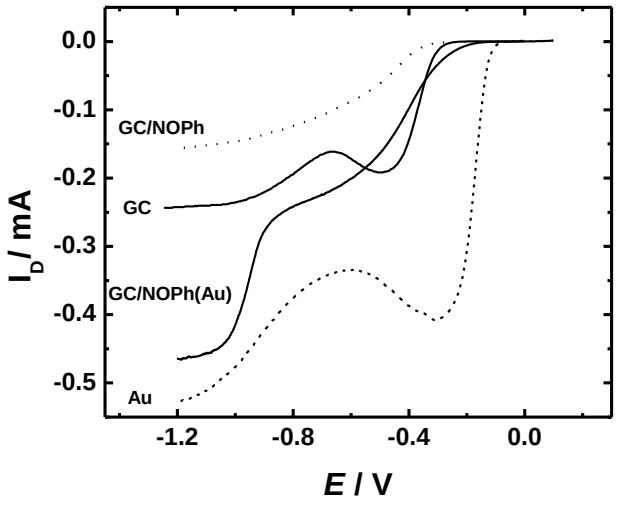
0.0
-0.1
-0.2
-0.3
-0.4
-0.5
GC/NOPh
GC
GC/NOPh(Au)
Au
ID / mA
-1.2
-0.8
-0.4
0.0
E / V

Fig. 9(a).

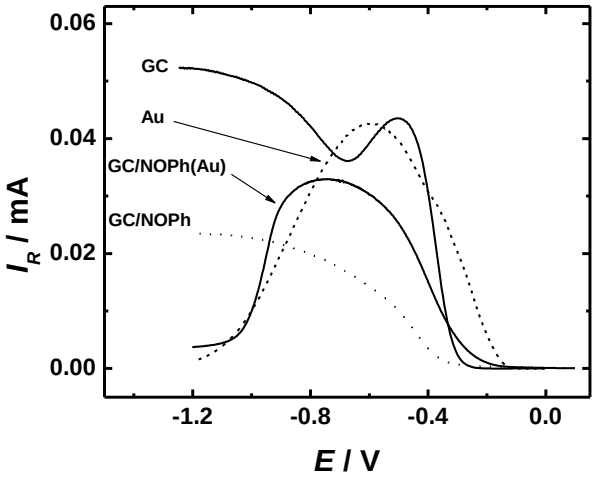
0.06
0.04
0.02
0.00
GC
Au
GC/NOPh(Au)
GC/NOPh
I_R / mA
-1.2
-0.8
-0.4
0.0
E / V

Fig. 9(b).

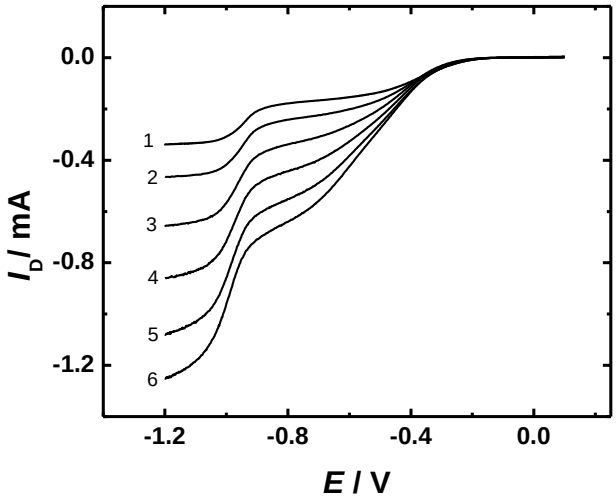
0.0
-0.4
-0.8
-1.2
1
2
3
4
5
6
I_D / mA
-1.2
-0.8
-0.4
0.0
E / V

Fig. 10.

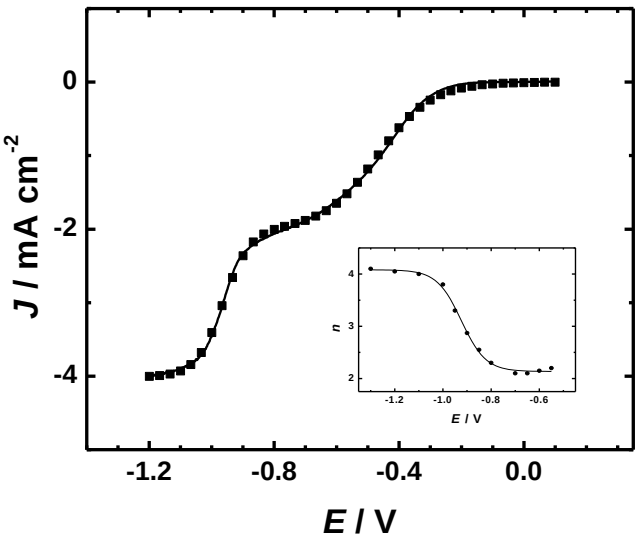

Fig. 11.